Doppler Dimming and Brightening Effects in Solar Prominences

Aaron W. Peat,[1,2]★ Christopher M. J. Osborne,[1] and Petr Heinzel[2,3]

[1]*SUPA School of Physics and Astronomy, University of Glasgow, Glasgow, G12 8QQ, UK*

[2]*University of Wrocław, Centre of Scientific Excellence – Solar and Stellar Activity, Kopernika 11, 51-622 Wrocław, Poland*

[3]*Astronomical Institute, Czech Academy of Sciences, 25165 Ondřejov, Czech Republic*

ABSTRACT

We explored the impact that Doppler dimming and brightening effects from bulk motions of solar prominences have on the formation of Ly α, H α, and Mg II h line profiles. We compared two schemes in which these effects manifest; when the prominence is moving radially away from the solar surface (radial case), and when the prominence is moving parallel to the solar surface (horizontal case). To do this, we analysed 13,332 model profiles generated through the use of the 1D NLTE (i.e. departures from Local Thermodynamic equilibrium) radiative transfer (RT) code PROMWEAVER, built on the LIGHTWEAVER NLTE RT framework to mimic the behaviour and output of the 1D NLTE RT code PROM. We found that horizontal velocities are just as, or more important than radial velocities. This demonstrates that horizontal velocities need to be accounted for when attempting to do any sort of forward modelling.

Key words: Sun: filaments, prominence – radiative transfer – line: profiles

1 INTRODUCTION

Solar prominences are cool, dense structures suspended in the solar corona which have been observed for centuries (e.g. Vassenius 1733; Secchi 1875; Hale 1929; Vyssotsky 1949) and simulated for half a century (e.g. Ishizawa 1971; Heasley et al. 1974; Heinzel et al. 1987; Gouttebroze 2004). It has been long shown that eruptive prominences are affected by Doppler dimming (DDE) and brightening (DBE) effects – where the incident radiation from the solar disc appears Doppler shifted in the frame-of-reference of the solar prominence, causing a brightening or dimming effect in the scattered line radiation. From here, we will use the acronym DXE to refer to both DDE and DBE. The former occurs when the incident radiation is in emission, and the latter when in absorption (Hyder & Lites 1970; Heinzel & Rompolt 1987; Labrosse et al. 2010; Vial & Engvold 2015).

More generally, when a prominence undergoes some bulk motion, DBE occurs when the incident radiation increases in the wavelength range of the absorption profile of the line in question, and DDE occurs when the incident radiation decreases in the wavelength range of the absorption profile of the line (Tandberg-Hanssen 1995).

An underexplored avenue which produces DXE is when a prominence has zero radial velocity, but non-zero velocity parallel to the solar surface (e.g. Rompolt 1967; Morimoto & Kurokawa 2003). We believe that no large scale quantitative study has been performed to understand the impact of such a velocity field on the radiation observed from solar prominences. In the case of prominences, this is commonly referred to as line-of-sight (LOS) velocity – however, in observations, true LOS velocities commonly contain some radial component. Here, we wish to demonstrate that, even with a zero

radial velocity component, prominences (and filaments) undergoing bulk motions experience significant DXE.

To begin, we will briefly introduce the NLTE (i.e. departures from Local Thermodynamic equilibrium) radiative transfer (RT) code which we use to simulate solar prominence emission. Following this, we briefly discuss our results and compare them to the effect when caused by non-zero radial velocities. We then discuss the implications this has for NLTE inversions of solar prominence atmospheres. Finally, we offer our conclusions.

2 PROMWEAVER

To demonstrate how non-zero velocities parallel to the solar surface in solar prominences produce DXE, we employ the use of the 1D NLTE RT code PROMWEAVER (Osborne 2022), built on top of the NLTE RT framework, LIGHTWEAVER (Osborne & Milić 2021). PROMWEAVER is written to efficiently and expediently replicate the results of the 1D NLTE RT code PROM (Gouttebroze et al. 1993; Heinzel et al. 1994; Labrosse & Gouttebroze 2004; Levens & Labrosse 2019). However, unlike PROM, PROMWEAVER has the ability to include any arbitrary bulk velocity field, meanwhile PROM can only include radial velocities. PROMWEAVER is not the first prominence code that can include arbitrary velocities; for example, MALI (Heinzel 1995; Heinzel et al. 2014) includes an implementation of the technique discussed in Heinzel & Rompolt (1987). However, in practice, it has only been used for radial velocities in the context of erupting prominences. Additionally, PROM produces half line profiles which are mirrored to produce the full profiles, but PROMWEAVER synthesises the entire line profile handling arbitrary velocity fields and interactions between overlapping transitions.

PROMWEAVER allows us to simulate any of the commonly modelled and observed lines; here we focus on Ly α, H α, and Mg II h using a

★ E-mail: aaron.peat@uwr.edu.pl
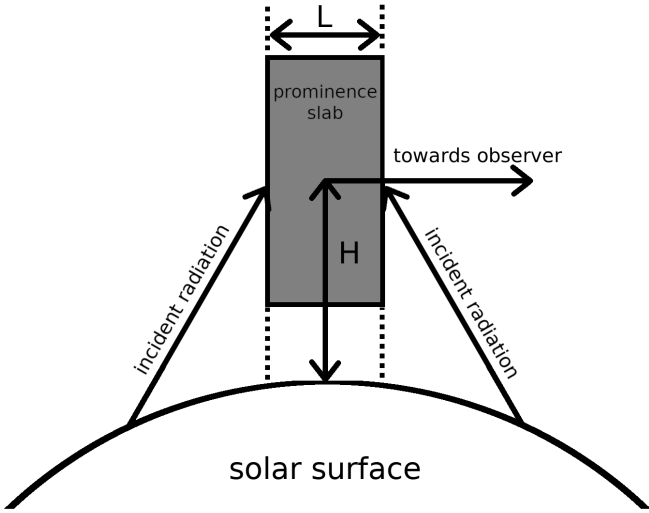
Figure 1. How PROM and PROMWEAVER model a prominence. Where H is the altitude of the prominence, and L is the slab width. This figure is adapted from Peat (2023).

Parameter	Unit	Iso Models	PCTR Models
T_{cen}	kK	8	6
T_{tr}	kK	–	100
p_{cen}	dyn cm^{-2}	0.05	0.1
p_{tr}	dyn cm^{-2}	–	0.01
L	km	400	407.69[a]
M	g cm^{-2}	2×10^{-6} [a]	5×10^{-6}
v_T	km s^{-1}	5	5
γ		–	4

Table 1. The base model parameters. For the isothermal and isobaric (iso) models, T_{cen} and p_{cen} are taken as T and p, respectively. The iso models are built using the slab width, while the PCTR models use maximum column mass to limit the extent of the structure.

[a] For this model type, this parameter is not strictly an input. It instead is found when solving statistical equilibrium.

5-level plus continuum H model and a 10-level plus continuum Mg model, following Leenaarts et al. (2013). Partial frequency redistribution (PRD) is of critical importance to the formation of the Ly α line (Heinzel et al. 1987). Additionally, PRD plays a key role in the formation of the Mg II resonance lines (Paletou et al. 1993; Heinzel et al. 2014), but this only affects the far wings of the emission, which may be below the detection limit (Heinzel et al. 2014). Here we treat all resonance lines in PRD. These atoms are solved simultaneously, allowing for mutual radiative interactions to occur.

PROMWEAVER, like PROM or MALI, models a solar prominence as a monolithic slab suspended in the solar corona (see Figure 1). It solves for statistical equilibrium of the considered atoms in the given slab, additionally conserving charge, and modifying the mass density of the structure to follow the prescribed pressure stratification (which is affected by ionisation). PROMWEAVER can use one of two model atmospheres; isothermal and isobaric, and one with a prominence-to-corona transition region (PCTR). The PCTR is the region where the cool and dense prominence transitions into the hot and tenuous corona. This region is modelled by the following equations (Kippenhahn & Schlüter 1957; Anzer & Heinzel 1999; Labrosse & Gouttebroze 2004),

$$T(m) = T_{cen} + (T_{tr} - T_{cen}) \left(1 - 4\frac{m}{M}\left(1 - \frac{m}{M}\right)\right)^{\gamma}, \quad (1)$$

$$p(m) = 4p_c \frac{m}{M}\left(1 - \frac{m}{M}\right) + p_{tr}, \quad (2)$$

for $\gamma \geq 2$, and where $p_c = p_{cen} - p_{tr}$. Here m is the column mass, M is the total column mass, $T(m)$ is the temperature as a function of column mass, T_{cen} is the central (prominence) temperature of the plasma, T_{tr} is the (coronal) temperature at the edge of the PCTR, and γ is a dimensionless factor that defines the extent of the PCTR. $p(m)$ is the pressure as a function of column mass, p_{cen} is the central (prominence) pressure, and p_{tr} is the (coronal) pressure at the edge of the PCTR. Eq. 1 is an empirical expression described in Anzer & Heinzel (1999), while Eq. 2 is an analytical formula from the Kippehahn-Schlüter model (KS; Kippenhahn & Schlüter 1957; Heasley & Mihalas 1976) for magnetohydrostatic (MHS) equilibrium. These equations are used as PROMWEAVER is built to mimic

PROM and this is how the PCTR is constructed in PROM (Labrosse & Gouttebroze 2004). As Eq. 2 comes from MHS equilibrium, it should be stressed that the applicability of this model for erupting prominences is questionable.

The incident radiation is generated using the FAL C atmosphere (Fontenla et al. 1993) and 'light cone' method discussed in the appendix of Jenkins et al. (2023). The incident radiation at $\mu = 1$ (i.e. radially from the solar surface) in the lines considered is shown in Fig. 2. In all situations we employ fully angularly dependent boundary conditions including the effects of limb darkening (self-consistently in a plane-parallel approximation as per Jenkins et al. (2023)) and arbitrary prominence motions.

The emergent intensity is computed by a final pass through the model using the computed level populations and ratio of the PRD emission to absorption profiles. The cones in the boundary conditions are disabled to compute the radiation along a specific ray (rather than the spherical integrals used to solve the non-LTE problem). This method can handle arbitrary viewing angles through the prominence slab, including when it is partially back-lit against the solar disc.

Using PROMWEAVER, we generated a large grid of models. These models are all based on one of two base models, which can be seen in Table 1. For isothermal models, slab width (L) is an input and the mass density (M) is calculated when solving statistical equilibrium. Meanwhile, for the PCTR models, mass density is an input, and the slab width is calculated during the solving of statistical equilibrium. Due to these differences, we attempted to select variables such that the slab widths and mass densities of these model types were of similar orders of magnitudes. To investigate the effect of bulk motion on the line profiles, we create a modified set of these base models such that they have horizontal velocities in the range 0–80 km s^{-1} with a step size of 0.8 km s^{-1}. Another set was also created with radial velocities in the same range in order to directly compare the two effects. As DXE is affected by altitude (Rompolt 1967, 1980a,b,c), we further modified these models to include altitudes in the range 5–70 Mm with a step size of 2 Mm. These combinations resulted in a total of 13,332 models.

These models were generated on a 36-core/72-thread dual socket motherboard machine with two Intel Xeon Gold 6140s with a base clock speed of 2.30 GHz, and a turbo speed of 3.70 GHz. The wall
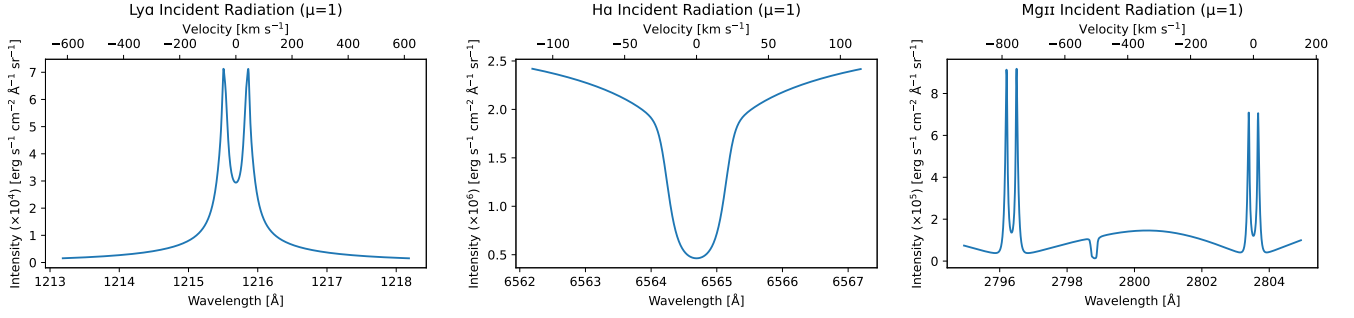
Figure 2. The incident radiation of Ly α, H α, and Mg II h&k as seen by the prominence for $\mu = 1$ (in the frame of the prominence, i.e. the radiation that would be incident on the prominence from directly below). In the Mg II h&k panel, the velocities are calculated using Mg II h (2803.53 Å) as the rest wavelength.

time[1] taken to produce the 13,332 models was approximately 70 hours with a CPU time[2] of approximately 5,000 hours.

3 RESULTS

DXE is effectively produced when a prominence undergoes some sort of bulk motion, causing the incident radiation to appear Doppler shifted in the frame of the prominence. For incident radiation seen in absorption, this causes a DBE as the shifted wings of the incident line profile increase the radiation scattered by the prominence. For incident radiation seen in emission, the wings also illuminate the prominence, but since the incident wings are dimmer than the incident line core, the net incident radiation is decreased and a DDE is observed. With double peaked emission profiles, at low velocities, we expect to see a DBE as the horns of the incident radiation are now impacting the outgoing radiation. At higher velocities, the wings of incident line profiles take precedence resulting in a DDE.

All 13,332 of our statistical equilibrium calculations successfully converged. The general relationships between velocity and height for the different model atmospheres and velocity types can be seen in Figs. 3 and 4. A value of 40 km s^{-1} was chosen as the fixed velocity for Fig. 3 simply because it was the middle of our velocity grid. A value of 11 Mm was chosen as the fixed altitude for Fig. 4 as altitudes of the order of 10 Mm are commonly used in papers which use PROM (e.g. Zhang et al. 2019; Levens & Labrosse 2019; Ruan et al. 2019; Peat et al. 2021). Due to our step size, however, the closest altitude to 10 Mm was 11 Mm.

Fig. 3 shows how the wavelength integrated intensity of the emission changes with altitude. The irregularities in the Ly α curves here are simply due to numerical errors because of a slight misalignment between the wavelength grids of the incident radiation and the emitted radiation from the prominence. Unsurprisingly, as the height increases, the integrated intensity falls – the Sun presents a smaller solid angle to the prominence. As the height increases the radial velocity curves were expected to produce a greater DXE effect than in the horizontal case. This is due to the lessening of the horizontal component of the incident rays as height increases. However, Mg II h does not exhibit this behaviour until higher altitudes. H α and Ly α both appear to diverge instead, with the two curves for Ly α in an isothermal and isobaric atmosphere appearing essentially parallel.

The integrated intensities of the lines in PCTR atmospheres are almost three times higher than in isothermal and isobaric atmospheres for the Hydrogen lines, and approximately only 10 per cent higher in Mg II h.

Fig. 4 shows how the integrated intensity of the emission changes with velocity for a fixed altitude. In H α, for both atmosphere types, radial and horizontal velocities produce a similar brightening effect in both behaviour and value. For Ly α and Mg II however, we see much more complicated behaviour. Up to 30 km s^{-1}, horizontal velocities produce a much larger DBE in Mg II h than the radial velocities. At higher velocities, the horizontal velocities also produce a much greater DDE than radial. The behaviour of Mg II in the radial case is consistent with that found by Heinzel et al. (2014). Ly α sees a similar effect, but only in the isothermal and isobaric atmosphere with the horizontal velocity dimming at a much greater rate than the radial velocity after its peak brightening. In the PCTR atmosphere, there is a similar, but much less pronounced, relationship.

The asymmetry of the lines was briefly investigated. Gontikakis et al. (1997) showed that when treated in PRD, the Ly α line profiles from moving solar prominences are asymmetric. This is not possible under CRD, and another reason why we treated all of the resonance lines in PRD. Here, the asymmetry was calculated via the quantile method (Kerr et al. 2015). This works by calculating the cumulative distribution function (CDF) of a line profile, and normalising them such that the values in the function range from 0–1. The wavelength at which the CDF is 0.5 (λ_{50}) is defined as the line core. If the line is of a Gaussian shape, the difference between λ_{88} and λ_{12} is the full width half maximum. From this, we calculate the asymmetry by the following relationship,

$$\text{Asymmetry} = \frac{(\lambda_{88} - \lambda_{50}) - (\lambda_{50} - \lambda_{12})}{\lambda_{88} - \lambda_{12}} = \frac{\lambda_{88} - 2\lambda_{50} + \lambda_{12}}{\lambda_{88} - \lambda_{12}}, \quad (3)$$

where a positive asymmetry means there is more emission in the blue, and a negative asymmetry means there is more emission in the red. The asymmetry in all of the line profiles is not appreciably affected in either the horizontal or radial velocity modes, never exceeding ±0.02. However, in observations, asymmetry is usually measured on the order of ±0.5 (Ruan et al. 2018; Peat et al. 2021). Therefore, this effect would be negligible in observations and cannot be a source of the asymmetry on its own.

4 DISCUSSION

The way in which DXE occurs in the radial and horizontal velocity cases are subtly different. In the much studied radial case, as the

---

[1] Real world time (i.e. measured on a clock on the wall).
[2] The total time contributed by all CPU threads.
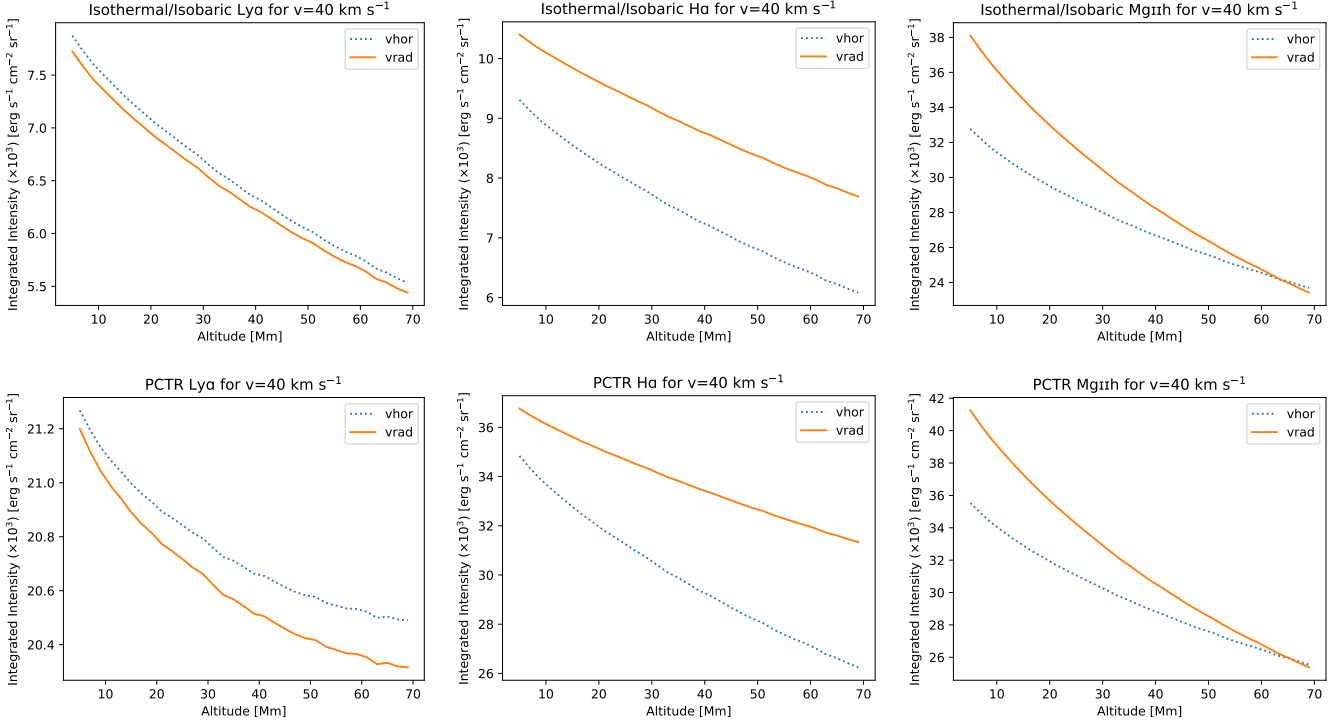
Figure 3. How DD/DB effects from horizontal (vhor) and radial velocities (vrad) are affected by a change in height. The top row is the results from the isothermal and isobaric atmospheres, and the bottom the PCTR atmospheres.
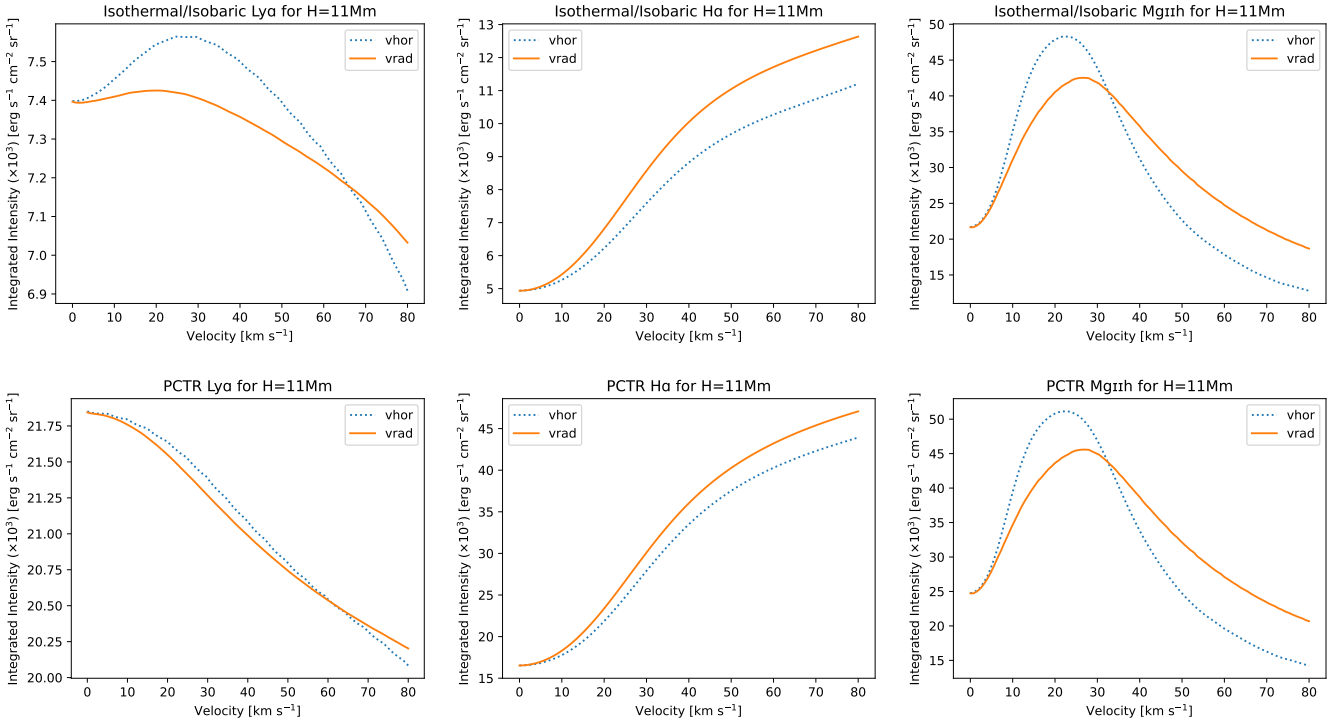
Figure 4. How DD/DB effects from horizontal (vhor) and radial velocities (vrad) are affected by a change in velocity. The top row is the results from the isothermal and isobaric atmospheres, and the bottom the PCTR atmospheres.

prominence moves away from the solar surface, the incident radiation appears red-shifted in the frame of the prominence, and if it is moving towards the the solar surface, the radiation appears blue-shifted. However, for the horizontal case, the leading edge of the prominence sees the incident radiation as blue-shifted, while the trailing edge sees the incident radiation as red-shifted. The radial case is only affected by one side of the wings of the incident radiation, whereas the horizontal case is affected by both sides of the wings.

The shape and intensity of the incident radiation profiles is extremely important to the total intensity of the line profiles produced by a prominence whether it is undergoing some bulk motion or not. Here we used the Ly α, H α, and Mg II h emission from the aforementioned FALC atmospheric model as the incident radiation. Whereas other studies modelling the emission from prominences use observations of the lines in question (e.g. Heinzel & Rompolt 1987; Levens & Labrosse 2019). However, if the incident radiation were to change from FALC to that found in observations, the qualitative relationships between the intensities and velocities would remain the same.

Much of the focus of DXE has been contextualised in the form of eruptive prominences moving predominantly radially (e.g. Heinzel & Rompolt 1987; Vial & Engvold 2015; Zhang et al. 2019), but this work shows that horizontal velocities also play a role. In observation, eruptive prominences are never going to erupt perfectly perpendicular to the solar surface. This will introduce a small horizontal component to its velocity, which is when the horizontal effect is at its greatest for lines with incident radiation in emission (see Fig. 4). Fig. 3 shows that radial and horizontal DXE appear to dissipate with height at the same rate, illustrating that this horizontal component will continue to be important as the prominence moves away from the solar disc. Furthermore, it is likely that the solar spectra incident on an erupting prominence are no longer symmetrical, increasing the complexity of the DXE effect. If it is assumed that an erupting prominence only has radial velocity, the radial velocity will be overestimated to account for the DXE introduced by the horizontal effect.

5 CONCLUSIONS

In this study we demonstrated an application of the NLTE Lightweaver RT framework, in the context of Promweaver, to explore DXE caused by different orthogonal motions. To meet this goal, we generated 13,332 models of differing parameters.

We showed the importance of all translational bulk motions of solar prominences on the formation of observed line profiles. Past studies mainly focused on radial velocities to better understand erupting prominences, but neglected horizontal velocities entirely. This neglect may have caused derived radial velocities of eruptive prominences from forward modelling to be overestimated.

In both the isboaric/isothermal and PCTR atmospheres, Ly α and Mg II h, as velocity increases, the horizontal case produces a much stronger DXE effect than its radial counterpart, but H α sees the greater effect caused by the radial case. With respect to increasing altitude, the intgrated intensities in the radial and horizontal cases both appear to diminish at equivalent rates in the two hydrogen lines. However, with respect to Mg II h, the radial and horizontal cases converge. Perhaps at larger velocities, Ly α and H α will also display this behaviour. In general, the magnitude of the DXE produced by the horizontal case is comparable to that produced in the radial case. In future studies, care should be taken when forward modelling to account for effects introduced by horizontal velocities and not to erroneously attribute it to only radial velocities.

DATA AVAILABILITY

This research presented an application of version 0.1.1 of Promweaver available at https://doi.org/10.5281/zenodo.6546897. The most recent version of Promweaver is available to download via pip or at https://github.com/Goobley/Promweaver.

All of the models used in this study can be found in the form of a Python pickle at https://doi.org/10.5281/zenodo.12083238.

REFERENCES

Anzer U., Heinzel P., 1999, Astronomy & Astrophysics, 349, 974
Fontenla J. M., Avrett E. H., Loeser R., 1993, ApJ, 406, 319
Gontikakis C., Vial J. C., Gouttebroze P., 1997, A&A, 325, 803
Gouttebroze P., 2004, Astronomy & Astrophysics, 413, 733
Gouttebroze P., Heinzel P., Vial J.-C., 1993, Astronomy & Astrophysics, 99
Hale G. E., 1929, ApJ, 70, 265
Harris C. R., et al., 2020, Nature, 585, 357
Heasley J. N., Mihalas D., 1976, ApJ, 205, 273
Heasley J. N., Mihalas D., Poland A. I., 1974, The Astrophysical Journal, 192, 181
Heinzel P., 1995, A&A, 299, 563
Heinzel P., Rompolt B., 1987, Sol. Phys., 110, 171
Heinzel P., Gouttebroze P., Vial J. C., 1987, Astronomy & Astrophysics, 183, 351
Heinzel P., Gouttebroze P., Vial J.-C., 1994, Astronomy & Astrophysics, 292, 656
Heinzel P., Vial J.-C., Anzer U., 2014, Astronomy & Astrophysics, 564, A132
Hunter J. D., 2007, Comp. Sci. Eng., 9, 90
Hyder C., Lites B., 1970, Solar Physics, 14
Ishizawa T., 1971, PASJ, 23, 75
Jenkins J. M., Osborne C. M. J., Keppens R., 2023, A&A, 670, A179
Kerr G. S., Simões P. J. A., Qiu J., Fletcher L., 2015, Astronomy & Astrophysics, 582, A50
Kippenhahn R., Schlüter A., 1957, Z. Astrophys., 43, 36
Labrosse N., Gouttebroze P., 2004, The Astrophysical Journal, 617, 614
Labrosse N., Heinzel P., Vial J.-C., Kucera T., Parenti S., Gunár S., Schmieder B., Kilper G., 2010, Space Science Reviews, 151, 243
Leenaarts J., Pereira T. M. D., Carlsson M., Uitenbroek H., De Pontieu B., 2013, The Astrophysical Journal, 772, 89
Levens P. J., Labrosse N., 2019, Astronomy & Astrophysics, 625, A30
Morimoto T., Kurokawa H., 2003, PASJ, 55, 503

Osborne C. M. J., 2022, Goobley/Promweaver: v0.1.1, doi:10.5281/zenodo.6546897, https://doi.org/10.5281/zenodo.6546897

Osborne C. M. J., Milić I., 2021, The Astrophysical Journal, 917, 14

Paletou F., Vial J. C., Auer L. H., 1993, Astronomy & Astrophysics, 274, 571

Peat A. W., 2023, PhD thesis, University of Glasgow, UK

Peat A. W., Labrosse N., Schmieder B., Barczynski K., 2021, Astronomy & Astrophysics, 653, A5

Rompolt B., 1967, Acta Astron., 17, 329

Rompolt B., 1980a, Hvar Observatory Bulletin, 4, 39

Rompolt B., 1980b, Hvar Observatory Bulletin, 4, 49

Rompolt B., 1980c, Hvar Observatory Bulletin, 4, 55

Ruan G., Schmieder B., Mein P., Mein N., Labrosse N., Gunár S., Chen Y., 2018, The Astrophysical Journal, 865, 123

Ruan G., Jejčič S., Schmieder B., Mein P., Mein N., Heinzel P., Gunár S., Chen Y., 2019, The Astrophysical Journal, 886, 134

Secchi A., 1875, Le Soleil. Gauthier-Villars, doi:10.3931/e-rara-14748

Tandberg-Hanssen E., 1995, The Nature of Solar Prominences. Astrophysics and Space Science Library Vol. 199, Springer Netherlands, Dordrecht, doi:10.1007/978-94-017-3396-0, http://link.springer.com/10.1007/978-94-017-3396-0

The Astropy Collaboration et al., 2013, Astronomy & Astrophysics, 558, A33

The Astropy Collaboration et al., 2018, The Astronomical Journal, 156, 123

Vassenius B., 1733, Philosophical Transactions of the Royal Society of London, 38, 134

Vial J.-C., Engvold O., eds, 2015, Solar Prominences. Astrophysics and Space Science Library Vol. 415, Springer International Publishing, Cham, doi:10.1007/978-3-319-10416-4, http://link.springer.com/10.1007/978-3-319-10416-4

Vyssotsky A. N., 1949, Meddelanden fran Lunds Astronomiska Observatorium Serie II, 126, 3

Zhang P., Buchlin É., Vial J.-C., 2019, Astronomy & Astrophysics, 624, A72

This paper has been typeset from a TEX/LATEX file prepared by the author.